

Unexpected Strength of Noble Gas Solids in Diamond Anvil Cells

Hui Liang, Nan Min, Di Wang, Xianqi Song, Pengyue Gao,* and Quan Li*



Cite This: *J. Phys. Chem. C* 2024, 128, 4839–4847



Read Online

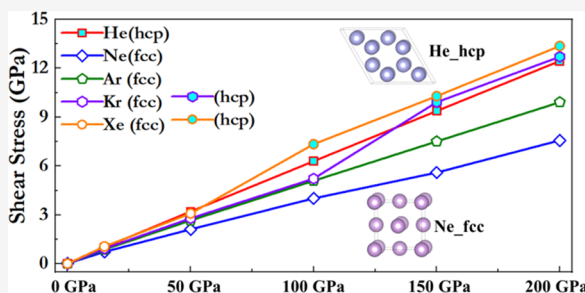
ACCESS |

Metrics & More

Article Recommendations

Supporting Information

ABSTRACT: The stress state inside a diamond anvil cell (DAC) during high-pressure experiments involves a diverse combination of six-dimensional uniaxial shear and compressive strains, ultimately generating a complex and nonhydrostatic state. To ensure experiments are performed under (quasi-)static pressure conditions, noble gases (NGs) are usually used as pressure transmission media (PTMs). Here, this study comprehensively investigates the ultimate mechanical strength of NG solids at high pressures using first-principles calculations; specifically, this study examines the stress response of NGs under shear strains to determine nonhydrostatic pressures that may be created when NG solids are used as PTMs in high-pressure experiments. Our results show that NG solids can provide good hydrostatic conditions for samples at relatively moderate pressures, while nonhydrostatic pressure inside DAC would be widespread and nonignorable under ultrahigh high-pressure conditions. Our results theoretically indicate that during high-pressure experiments, He is an ideal candidate as a PTM under relatively low-pressure conditions (<15 GPa), but Ne shows the best performance at higher pressure. The current work offers insights into the fundamental structural and physical properties of the NG solids and enriches a fundamental understanding of the nonhydrostatic effects of broadly defined strains on modulating the physical and chemical properties of functional materials.



INTRODUCTION

Pressure, as a fundamental thermodynamic variable, can regulate the properties of materials by changing the atomic and electronic structure of matter, realizing various new materials with novel properties that are inaccessible under ambient conditions.^{1–7} Under high pressure, noble gases (NGs), especially krypton (Kr) and xenon (Xe), can form several thermodynamically stable compounds because of their large atomic radii and the relatively weak binding ability of their atomic nuclei to the outermost electrons. These findings have challenged the prevailing understanding that NGs are always chemically inert because of their stable closed-shell electron configuration, which has stimulated subsequent theoretical and experimental exploration of NGs.^{8–13} Pressure has a certain regulatory effect on the configuration of the outermost electrons of NGs, i.e., it changes the electronic states and interatomic electrostatic interactions of NGs, which therefore exhibit unique physical and chemical properties.^{14–25} In contrast, helium (He), neon (Ne), and argon (Ar), with atomic radii much smaller than those of Kr and Xe, do not undergo structural phase changes within a wide temperature and pressure range, especially at high temperature and pressures.

A diamond anvil cell (DAC) is used to generate high pressure in experiments to study the evolution of the structure and physical and chemical properties of materials. To obtain more accurate experimental results, pressure transmission media (PTMs) are usually used in high-pressure experiments

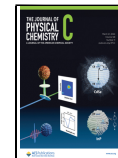
to ensure the experiment is performed under (quasi-)hydrostatic pressure conditions. Notably, the realization of a (quasi-)hydrostatic pressure environment inside the DAC depends on the targeted sample, experimental measurement methods, and PTMs, where the last factor plays a crucial role. Most PTMs, such as methanol–ethanol mixtures, methanol–ethanol–water mixtures, silicone oil, nitrogen, and NGs,²⁶ provide good quasi-hydrostatic pressure conditions under relatively moderate pressure. Among the PTMs given above, NGs have the most superior hydrostaticity. Hydrostatic pressure is defined as the stress states of an equilibrium structure in which the diagonal components of stress tensors (normal stress) are equal and the off-diagonal stress components (shear stress) are zero, while nonhydrostatic pressure generates when the stress tensors do not satisfy the above conditions. At a required pressure, the stress state inside the DAC is uncertain because it may involve different combinations of hydrostatic pressure and additional uniaxial shear or compressive strain, ultimately forming a nonhydrostatic state inside the DAC. The chemical properties of He, Ne, and Ar are relatively stable, and they do not easily

Received: February 10, 2024

Revised: February 29, 2024

Accepted: March 1, 2024

Published: March 12, 2024



react with diamonds and gaskets. Thus, they are widely used as PTMs in high-pressure experiments.²⁷ Among the above-given PTMs, He is the most attractive PTM, which is attributed to its highest solidification pressure (11.8 GPa at 298 K) and the release of internal stress through recrystallization after solidification under high pressure.²⁸ Furthermore, He generates a very weak parasitic X-ray diffraction signal during experimental measurements.²⁹ Therefore, NGs with smaller radii, such as He and Ne, are considered satisfactory PTMs and can create good quasi-hydrostatic conditions over a wide pressure range.

Previous experimental work has shown that the presence of nonhydrostatic pressure in DAC inevitably leads to deviations between experimental and theoretical results and that the presence of nonhydrostatic pressure can greatly affect the results.³⁰ The pressure generated by a DAC applied on the sample is inevitably anisotropic owing to solidification of the PTM, which has often been ignored. However, pressure-distribution models indicate that the shear stresses inside a DAC can reach 0.29–0.38Ps (Ps is the peak axial stress/pressure inside a DAC),^{31,32} i.e., there may be an inhomogeneous distribution of pressure in the transmission media. Experimentally, nonhydrostatic pressure affects the full-width at half-maximum of the ruby R1 and R2 fluorescence peaks and the R1–R2 splitting^{33,34} and also considerably affects the structure and properties of a material, e.g., nonhydrostatic stress affects the high-pressure phase structure of silicon,³⁵ affects the onset transition pressure of iron during the pressure-induced phase transformation process,³⁶ and accelerates the decrease in the superconducting transition temperature with pressure in MgB₂.³⁷ Although experimental studies have been reported on the use of the pressure gradient method and radial X-ray diffraction method to measure the mechanical strength of NG solids under pressure,^{33,38,39} it is still necessary to understand the ultimate mechanical strength of NGs under high pressures, and especially examine their stress response behavior under nonhydrostatic pressures to clarify nonhydrostatic pressures that may be created when NG solids are used as PTMs.

Herein, comprehensive computational studies were performed on NG solids at hydrostatic pressures of 0–200 GPa using first-principles calculations to examine their elastic moduli at small strains near the equilibrium and their stress–strain relations at large strains. Currently, the high-pressure experiments are generally performed within 200 GPa. We therefore chose the up limit of the pressure in this study as 200 GPa. These calculations aimed to determine the theoretical ultimate shear strength of NG solids, which can be indirectly defined as the nonhydrostatic pressure that may be created when NG solids are used as PTMs in high-pressure experiments. The stress response and corresponding structural deformation patterns of NG solids under shear and compressive strains were carefully analyzed to determine the influence of applied external stress on the structural stability and mechanical properties of NGs to evaluate nonhydrostatic stresses that may be generated when NG solids used as PTMs in high-pressure experiments. Calculated results show that Ne exhibits the lowest strength under both shear and compressive strains. The obtained lowest stress of NG solids reveals the following consistent stress sequence under shear and compressive deformations: Ne < Ar < He < Kr < Xe. Previous experimental work compared the hydrostaticity of several PTMs within 50 GPa, while our work emphasizes the

hydrostaticity of noble gases as PTMs at high pressures. And our calculations were performed at 0 K, without considering the influence of temperature effects. Therefore, this inconsistency between the current theoretical and experimental results may be induced by temperature effects.

■ METHODS

Structural relaxations, energy calculations, and stress–strain calculations were performed using the Vienna ab initio simulation package code⁴⁰ with the projector augmented wave method and Perdew–Burke–Ernzerhof generalized gradient approximation functional.⁴¹ An energy cutoff of 900 eV and a Monkhorst–Pack⁴² grid with a spacing of 0.2 Å⁻¹ were used to ensure the energy, stress, and force convergence to 1 meV/atom, 0.1 GPa, and 0.001 eV/Å, respectively. Phonon dispersions were calculated based on density functional perturbation theory with IBRION = 8, implemented in PHONOPY software⁴³ with forces obtained by the Hellmann–Feynman theorem. For the simulated hexagonal close-packed (hcp) phase and face-centered cubic (fcc) phase, we constructed 3 × 3 × 2 and 2 × 2 × 4 supercells with a total of 288 and 256 atoms, respectively. Elastic constants were calculated using the strain–stress method, and elastic moduli were derived from the Voigt–Reuss–Hill⁶³ averaging scheme. Stress–strain relations under shear and compressive loading conditions were determined using the well-developed method.^{44–52} At each step, a fixed strain was applied with a strain increment of 0.01, and the corresponding stress was determined. Moreover, the other five components of the Hellmann–Feynman stress tensors and atoms inside the unit cell were simultaneously relaxed until the residual forces and stresses were less than 0.005 eV/Å and 0.1 GPa, respectively. This approach described the stress response and associated structural deformation mode of the material over a large strain range, helping to determine the mechanical properties of the material. Long-range forces such as Van der Waals and three-body forces⁵³ are not considered in the current calculations, but these long-range forces effects could modify the reported results.

■ RESULTS AND DISCUSSION

The high-pressure phase diagram and the equation of state of NG solids were extensively investigated via experimental studies using the X-ray diffraction method and theoretical studies using density functional theory calculations.^{54–68} According to previously reported theoretical and experimental results, NGs exist in the fcc phase at ambient pressure and undergo a phase transition to the hcp phase as the pressure increases, except He, which already exists in the hcp phase at ambient pressure. Experimental studies at gigapascal pressures and theoretical studies at terapascal pressures show that He (experimental and theoretical analysis pressures = 58 GPa and 10 TPa, respectively) and Ne (208 GPa and 256 TPa) are stable in the hcp phase and fcc phase, respectively, over a wide pressure range. First-principle calculations based on the local density approximation show that the phase transitions of solid Ar and Kr from the fcc to hcp phase occur at 220 and 130 GPa, respectively. X-ray diffraction measurements of solid Xe indicate that it completes the phase transition from the fcc to the hcp phase at a pressure of ~137 GPa. The structural parameters and volumes of fcc and hcp phases of NGs were optimized under hydrostatic pressures of 0, 15, 50, 100, 150,

and 200 GPa, and the phase stability of NGs at pressures of 0–200 GPa is summarized in Figure 1a. The crystal structures of

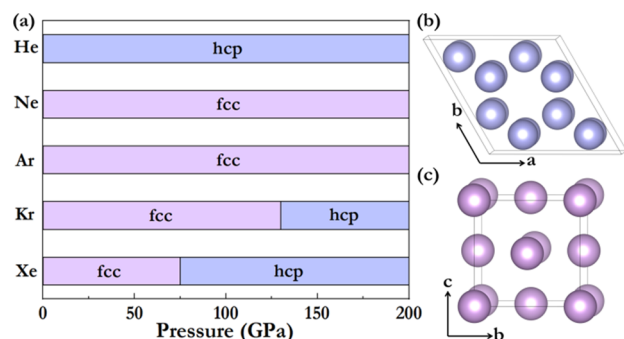


Figure 1. (a) Phase diagram of NGs at 0–200 GPa. (b) $P6_3/mmc$ (hcp) phase of He at 200 GPa. (c) $Fm-3m$ (fcc) phase of Ne at 200 GPa.

He (hcp phase) and Ne (fcc phase) are shown in Figure 1b and c, respectively. The optimized lattice parameters and volumes of NGs at 0–200 GPa are shown in Table S1,⁶⁹ and the obtained results are consistent with experimental data.

To gain insights into the elastic stability under external load, we evaluated elastic parameters of NG solids at 0–200 GPa. The resulting C_{ij} results at 200 GPa are summarized in Table S2.⁶⁹ Our calculated elastic parameters satisfy the Born–Huang criteria,⁷⁰ verifying that NG solids are mechanically stable at 200 GPa. Then, their shear modulus was obtained from the elastic parameters, which reflect the ability of NG solids to resist shear strain. The shear moduli of NG solids under hydrostatic pressures of 0–200 GPa are shown in Figure 2a, and the three-dimensional (3D) shear moduli of He and

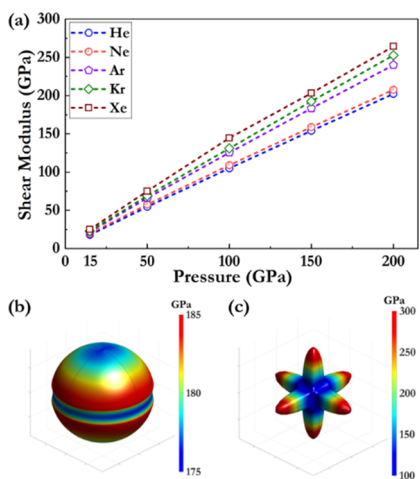


Figure 2. (a) Pressure dependence of the shear moduli of NG solids and (b,c) 3D spatial distribution of the shear moduli of He and Ne at 200 GPa.

Ne at 200 GPa are shown in Figure 2b and c, respectively. Calculated results show that the shear modulus of NG solids increases linearly with an increase in hydrostatic pressure and also increases with an increase in the atomic radius of NG. Notably, at a hydrostatic pressure of 200 GPa, the shear modulus of NG solids is approximately half that of diamond (443.0 GPa) at atmospheric pressure,⁷¹ indicating that NG solids can sustain shear deformations under high pressures.

The 3D shear moduli of He (hcp) and Ne (fcc) at 200 GPa were also visualized, respectively. For an isotropic system, the visualization of the 3D shear modulus is almost a perfect sphere. However, for an anisotropic system, the proportion of deviation from the sphere reflects the degree of anisotropy. Our results show that He (hcp) has a good isotropic response to shear deformation under small loads close to equilibrium [Figure 2b], while Ne (fcc) exhibits relatively large anisotropy [Figure 2c]. Since He and Ne have similar shear moduli, the weakest shear strength of Ne is much lower than that of He. Therefore, Ne has a lower upper limit of stress release inside the DAC, which can provide a better (quasi-)hydrostatic pressure environment for the sample.

Next, the mechanical strengths of NG solids under large strains were determined by calculating the stress–strain relations and examining their structural and stress responses under various shear and compressive deformations. The solidification pressures of He, Ne, Ar, Kr, and Xe at 298 K are 11.8, 4.8, 1.3, 0.8, and 0.4 GPa, respectively.⁷² Therefore, the stress–strain relations of NGs along different indicated crystallographic directions at 0, 15, and 200 GPa (i.e., close to the solidification pressure) and 50, 100, 150, and 200 GPa were studied. The shear stress–strain relations of NG solids with the lowest stress peak under different pressures are shown in Figure 3a–e, and the specific calculation details are shown in Figures S1–S5.⁶⁹ At 0–200 GPa, He, Ne, and Ar exist in hcp, fcc, and fcc phases, respectively, and Kr and Xe exhibit two types of stress–strain curves because of their phase transition from fcc to hcp phases. Our results indicate that the distinct atomic arrangements between the fcc and hcp phases lead to considerable differences in the stress–strain relations under shear conditions, although there is no clear evidence that chemical bonds are formed in NG solids. Specifically, the shear strain of the hcp lasts ~0.15, whereas that of the fcc lasts ~0.25, and the stress of the hcp is generally higher than that of the fcc, indicating that the sequence of shear stresses is Ne < Ar < He < Kr < Xe. The lowest shear stresses (i.e., ideal strength) of NGs under hydrostatic pressures of 0–200 GPa are summarized in Figure 3f, where the hcp and fcc phases of NGs are presented by solid and hollow symbols, respectively. Another remarkable feature of the calculated stress–strain relations of NG solids is the absence of sharp stress release and structural variations over the entire strain range, implying the great structural stability of NG solids throughout the straining process. This behavior is uncommon in molecular solids, as exemplified by hydrogen,⁷³ which exhibits a sudden and precipitous stress drop right after peak stress is reached. Instead, this behavior is similar to metals, such as copper and aluminum, which exhibit a creep-like stress response under various loading conditions.⁷⁴ The calculated results show that NG solids have a shear strength of 2–4 at 50 GPa, which is close to the strength of metallic aluminum or copper at atmospheric pressure,⁷⁴ and a shear strength of 4–7 at 100 GPa, which is close to the strength of the semiconductor silicon at atmospheric pressure.⁷⁵ These results show that NG solids can resist shear deformation at megabar pressures; i.e., NG solids cannot easily maintain hydrostatic properties inside the DAC at high pressures and cannot ensure a quasi-hydrostatic environment when they are used as PTMs at high pressures. Mao et al. experimentally showed that the strength of solid Ar considerably increases with an increase in pressure, where the shear strength of solid Ar exceeds 2.7 at 55.0 GPa.³⁹ The bulk shear strength t of solid Ar is defined as follows:

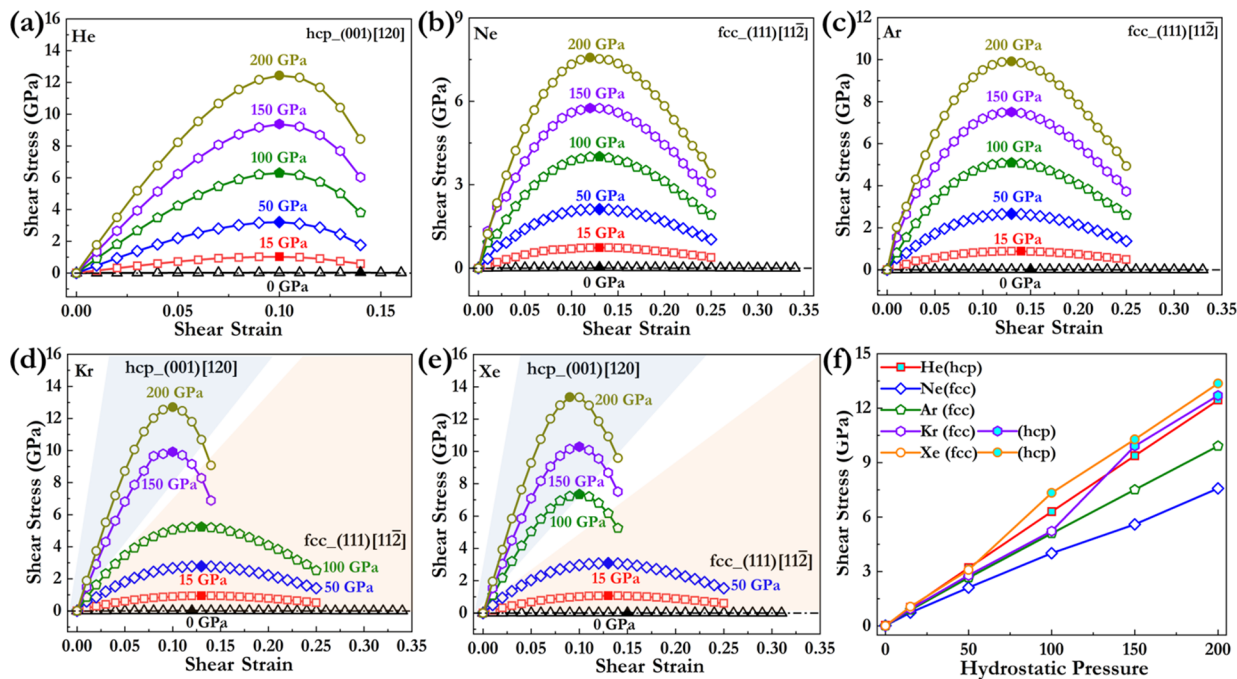


Figure 3. (a–e) Lowest shear stress response curves of NG solids at 0–200 GPa, and the corresponding ideal shear strength (lowest peak stress) is presented by solid symbols. (f) Summary of the ideal shear strength (lowest peak stress) of NG solids at 0–200 GPa. The ideal shear strengths for the hcp and fcc phases of NG solids are defined by the lowest peak stress along the (001)[120] and (111)[11–2] shear slip directions, respectively.

$$t = 6G < Q \quad (1)$$

where G is the shear modulus and Q is the magnitude of strain. $\langle Q \rangle$ is the average $Q(hkl)$ that can be obtained from the trigonometric function of d -spacing and φ , as follows:

$$d(hkl) = d_p(hkl)[1 + (1 - 3\cos 2\varphi)Q(hkl)] \quad (2)$$

which expresses the diffraction rings of solid Ar.^{38,39} Notably, solid Ar exhibits a shear strength of 2.6 at 50.0 GPa, according to calculations performed in this study, consistent with experimental results. Because the calculations in this study were performed at 0 K, there may be slight deviation from experimentally measured data. It is expected that theoretical and experimental results may become more consistent if the temperature effect is considered.

To gain insight into the high shear stress exhibited by NG solids under high pressures, their structural and stress responses under shear strains were closely analyzed (Figure 4). Because NGs are monatomic molecules with weak van der Waals forces, the change in the intermolecular distance of NG solids is used to characterize the structural changes in NG solids during the shearing process [Figure 4a–c]. Interestingly, the change in the intermolecular distance of NG solids is more pronounced in the hcp phase than in the fcc phase, which is consistent with the fact that the hcp phase has higher shear stress during straining than the fcc phase [Figure 3f]. Moreover, this phenomenon becomes more pronounced as the atomic radius of NGs increases, for example, He, Kr, and Xe exist in the hcp phases at 200 GPa, but the change in the intermolecular distance of Xe is more obvious than that of He and Kr [Figure 4c]. That is because Xe has the largest atomic radius (among the three) and its atomic nucleus has a weak attraction to its outermost electron, resulting in more notable structural deformation under shear strain. The structural snapshots of He in the hcp phase and Ne in the fcc phase at key strains of 200 GPa are shown in Figure 4d, where their

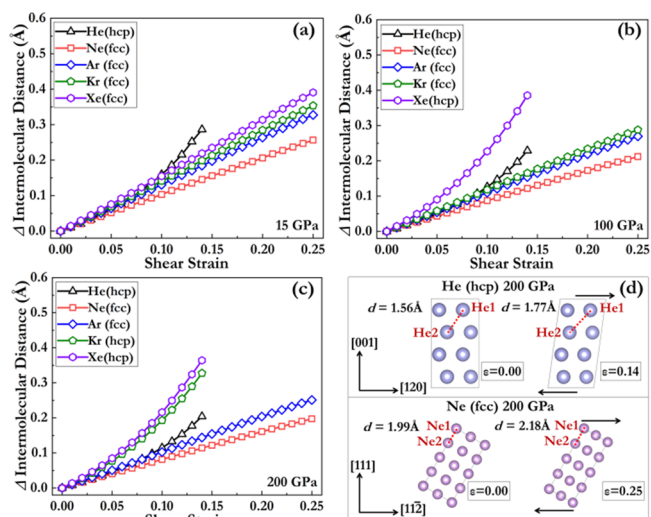


Figure 4. (a–c) Evolution of the intermolecular distances of NG solids under shear strains and (d) structural snapshots of He (hcp) and Ne (fcc) at key shear strains of 200 GPa. The arrows in (d) indicate the shearing direction.

structural deformation includes a slight deformation of the crystal lattice and movement of the relative positions of atoms. Our results show that Ne with an insignificant variation in the intermolecular distance has the lowest shear stress in the pressure range of 0–200 GPa.

The evaluation of structural and stress responses of NG solids under compressive strains at hydrostatic pressures of 0, 15, 50, 100, 150, and 200 GPa was also evaluated. Notably, the creep-like stress response of NG solids under shear strains discussed above is also observed under compressive strains, as shown in Figure 5. The stress–strain relationships with the lowest stress peak for He, Ne, Ar, Kr, and Xe are shown in

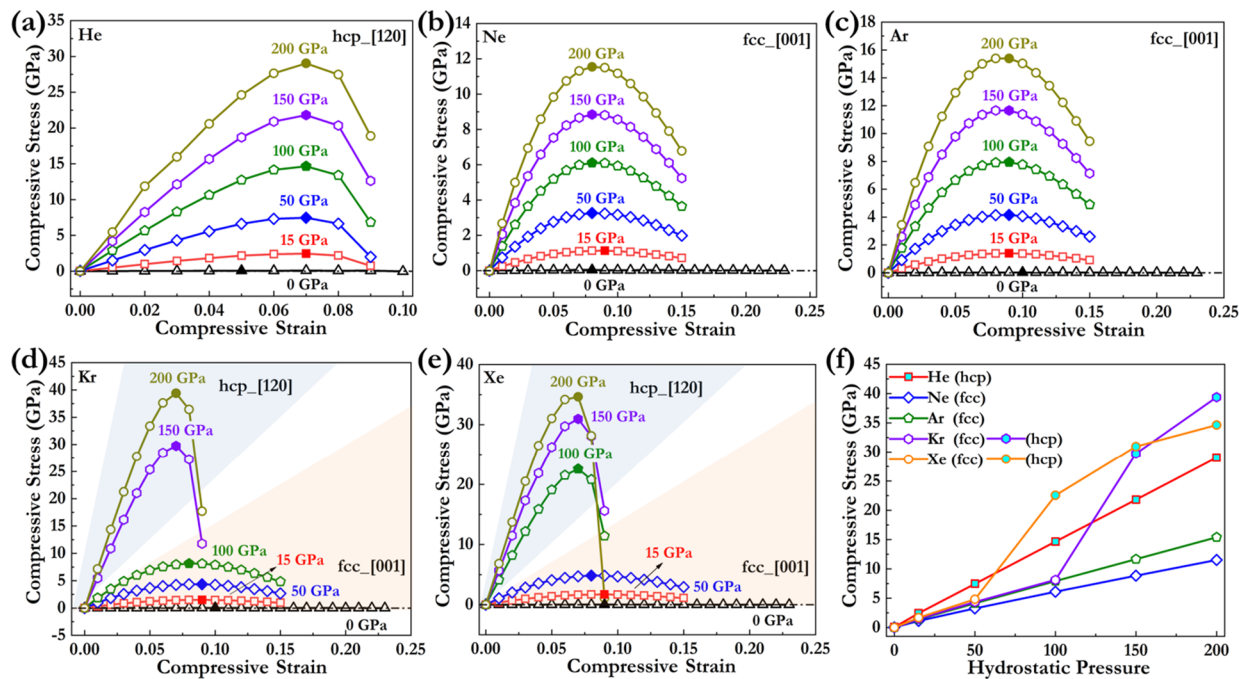


Figure 5. (a–e) Lowest compressive stress response curves of NG solids at 0–200 GPa, and the corresponding ideal shear strength (lowest peak stress) are presented by solid symbols. (f) Summary of the ideal compressive strength (lowest peak stress) of NG solids at 0–200 GPa. The ideal compressive strengths for the hcp and fcc phases of NG solids are defined by the lowest peak stress along the [120] and [001] compressive slip directions, respectively.

Figure 5a–e (see Figures S6–S10⁶⁹ for more details). The lowest compressive stresses (i.e., ideal strength) of NG solids are summarized in Figure 5f, where the hcp and fcc phases are represented by solid and hollow symbols, respectively. Figure 5 shows that the stress of the fcc phase under compressive strain is still lower than that of the hcp phase, consistent with the stress response under shear strain [Figure 3f]. Specifically, at 200 GPa, the compressive stresses of Ne and Ar in the fcc phase are 11 and 15 GPa, whereas that of He in the hcp phase is as high as 29 GPa. Therefore, the sequence of NGs according to compressive stresses is as follows: Ne < Ar < He < Kr < Xe. Moreover, the strain of the fcc phase is up to 0.15, whereas that of the hcp phase is 0.10, which means that the fcc phase can maintain the stability of the structure in a larger strain range. The contrasting results of the ductility of NG solids under shear (Figure 3) and compressive (Figure 5) deformation show that NG solids exhibit a higher degree of ductility under shear strains than under compressive strain, which means that NG solids can strongly sustain shear deformations, indicating their good structural stability under large strains.

Figure 6 shows the change in the intermolecular distances of NG solids under compressive deformations and structural snapshots of He and Ne at key strains of 200 GPa. An analysis of the change in the intermolecular distance of NG solids under compressive strains shows that NG solids undergo a considerably softened deformation mode, which is characterized by an incremental increase in the intermolecular distance over a large deformation range [Figure 6a–c]. Notably, compared with their undeformed structure, NG solids exhibit uniform structural deformation under compressive loading conditions, including an increase in the intermolecular distance and a slight deformation of the crystal lattice, which releases the stress in the system without strain

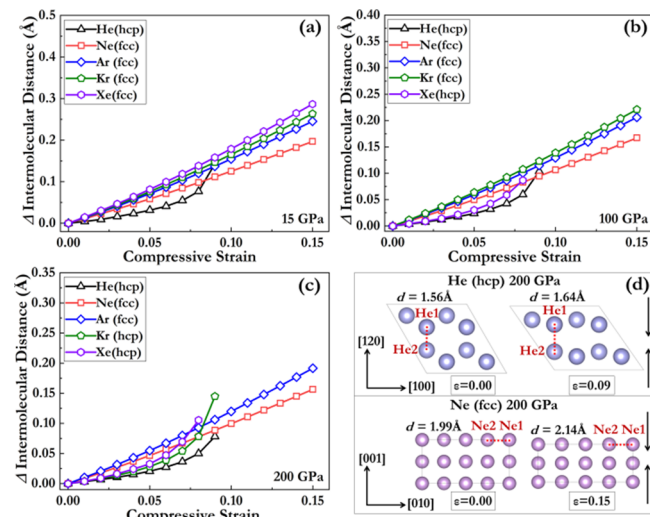


Figure 6. (a–c) Evolution of the intermolecular distances of NG solids under compressive strains and (d) structural snapshots of He (hcp) and Ne (fcc) at key compressive strains at 200 GPa. The arrows in (d) indicate the compression direction.

localization [Figure 6d]. Similarly, the fcc phase exhibits a more gentle structural variation than the hcp phase under compressive strain, consistent with the fact that the fcc phase has a lower compressive strength than the hcp phase. An analysis of the stress–strain response of NG solids under shear and compression shows that compared with strong covalent bonds the intermolecular force of NGs can make the structure more flexible under large strains and more conducive to resisting structural deformation. This intriguing stress–strain behavior of NG solids offers insights to indirectly evaluate the nonhydrostatic pressure generated when NG solids are used as

PTMs in high-pressure experiments, thereby understanding experimentally unexplained phenomena from a theoretical perspective.

More recent studies have explored the metallization and superconductivity of diamond and hydrogen under anisotropic stress, which drives the metallization of the diamond and hydrogen.^{46,73} As PTMs, it is necessary to understand the electronic properties variations of NG solids under nonhydrostatic pressure, which has important implications for understanding the measurement of electrical transport properties during high-pressure experiments. NG solids are monatomic molecular crystals with completely filled electronic shells and symmetrical charge distributions. Therefore, their metallization pressures are high. Diffusion quantum Monte Carlo (DMC) simulation and Kohn–Sham Generalized Gradient Approximation (GGA) calculation show that the metallization pressures of solid He are 25.7 and 17.0 TPa,⁵⁷ respectively. Moreover, first-principle simulations performed using the GW approximation and GGA approximations show that the metallization pressures of solid Ne are 176.0 and 142.0 TPa,⁶⁰ respectively. Theoretical studies indicated that the hcp structures of Ar and Kr undergo an insulator–metal transition at 510.0 and 310.0 GPa,⁶² respectively. Direct measurements of the electrical transport properties of Xe indicate that it exhibits metallic behavior at 130–155 GPa.^{65–67} To elucidate the effect of nonhydrostatic pressure on the electronic properties of NGs, the evolution of E_g under shear and compressive strains at 100 GPa was studied [Figure 7a,b]. The

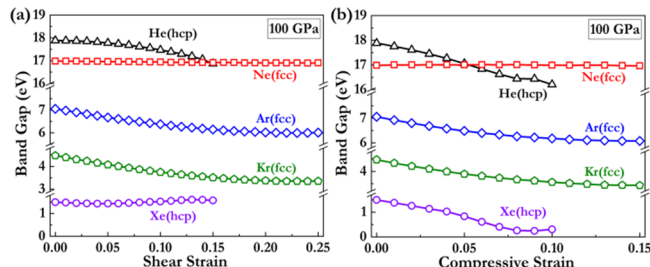


Figure 7. Electronic band gaps (E_g s) of deformed NG solids along (a) shear and (b) compressive paths at 100 GPa.

results show that E_g s of Ne hardly change during shear and compression deformation, and the changes of Ar and Kr are also slight, which is unlike E_g s of He and Xe, which decrease as strain increases. This indicates that the electronic properties of Ne are not affected by nonhydrostatic stress, consistent with our results that Ne is a more suitable PTM in high-pressure experiments than He.

A comparison of the shear strength (SS) of the NG solids with those of diamond, *c*-BN, and WC is shown in Figure 8a. The normalized results show that the shear strength of NG solids increases significantly with increasing pressure, indicating that it is sensitive to hydrostatic pressure. In addition, the ratio of NG solids to diamond, *c*-BN, and WC shear strength was calculated [Figure 8b–d]. As the typical superhard materials, diamond, *c*-BN, and WC are chosen to compare with the NG solids. The results show that as the hydrostatic pressure increases, the shear strength ratios of NG solids and three typical superhard materials increase significantly. In other words, the greater the hydrostatic pressure in the high-pressure experiment, the more nonnegligible the nonhydrostatic stress generated by the NG solids. In general, NG solids can provide

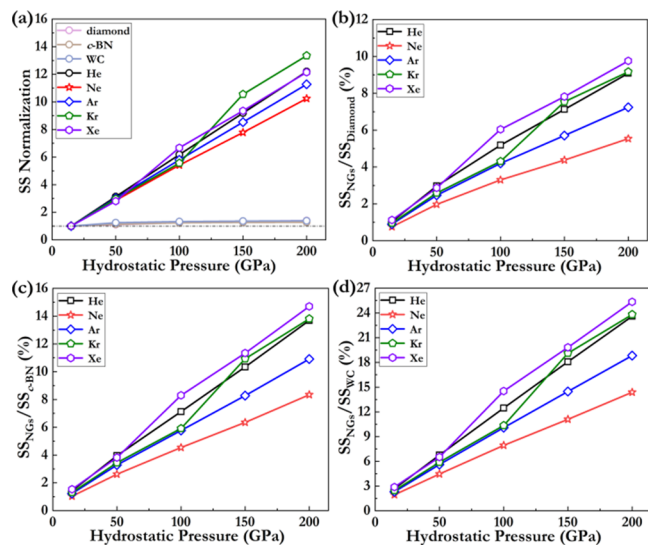


Figure 8. (a) SS normalization of NG solids, diamond, *c*-BN, and WC at 0–200 GPa. (b–d) SS ratio of NG solids to diamond, *c*-BN, and WC at 0–200 GPa.

excellent hydrostatic conditions for samples at relatively low pressures (i.e., before solidification, <15 GPa) and satisfactory hydrostatic conditions at moderate pressure (i.e., a maximum shear of about 3 at 50 GPa), but they generate nonnegligible anisotropic stress at higher pressures, resulting in nonhydrostatic environments for samples.

CONCLUSIONS

In summary, the structural stability and mechanical properties of NG solids under shear and compressive strains at high pressures have been systematically studied. Results show that NG solids exhibit unexpected mechanical stability at high pressures, including an extremely high elastic modulus near equilibrium and intrinsic resistance to structural deformations at large shear and compressive strains. All structural variations occur without precipitous change over a much-prolonged strain range, showing their great structural stability. Our calculations reveal that the unexpectedly high strengths of NG solids under large shear and compressive strains originated from their intrinsic electronic structures and special monatomic molecular structural characteristics. Compared with other liquid PTMs (e.g., methanol–ethanol mixtures and silicone oil) and solid PTMs (e.g., NaCl and pyrophyllite), NGs are the most commonly used PTMs in high-pressure experiments and have the best hydrostaticity. However, NG solids have a shear strength of 2–4 at 50 GPa, indicating that they will generate anisotropic stress at high pressures, resulting in nonhydrostatic environments for samples. Therefore, nonhydrostatic pressure inside DAC is widespread in high-pressure experiments. It can be theoretically concluded that Ne with an fcc structure exhibits excellent hydrostaticity and is more suitable as a PTM in high-pressure experiments than He. These findings have implications for understanding the application of NG solids as PTMs in high-pressure experiments. These results are also helpful for further exploration of NG solids under high pressure and provide theoretical knowledge for understanding NG elements under high pressure.

ASSOCIATED CONTENT

Supporting Information

The Supporting Information is available free of charge at <https://pubs.acs.org/doi/10.1021/acs.jpcc.4c00909>.

Detailed stress-strain relations of NG solids under shear and compressive strains along various indicated crystallographic directions at hydrostatic pressures of 0, 15, 50, 100, 150, and 200 GPa ([PDF](#))

AUTHOR INFORMATION

Corresponding Authors

Pengyue Gao — State Key Lab of Superhard Materials and Key Laboratory of Material Simulation Methods & Software of Ministry of Education, College of Physics, Jilin University, Changchun 130012, China; [orcid.org/0000-0003-1608-4934](#); Email: gpy@calypso.cn

Quan Li — State Key Lab of Superhard Materials and Key Laboratory of Material Simulation Methods & Software of Ministry of Education, College of Physics and International Center of Future Science, Jilin University, Changchun 130012, China; [orcid.org/0000-0002-7724-1289](#); Email: liquan777@jlu.edu.cn

Authors

Hui Liang — State Key Lab of Superhard Materials and Key Laboratory of Material Simulation Methods & Software of Ministry of Education, College of Physics, Jilin University, Changchun 130012, China

Nan Min — State Key Lab of Superhard Materials and Key Laboratory of Material Simulation Methods & Software of Ministry of Education, College of Physics and International Center of Future Science, Jilin University, Changchun 130012, China

Di Wang — State Key Lab of Superhard Materials and Key Laboratory of Material Simulation Methods & Software of Ministry of Education, College of Physics and International Center of Future Science, Jilin University, Changchun 130012, China

Xianqi Song — State Key Lab of Superhard Materials and Key Laboratory of Material Simulation Methods & Software of Ministry of Education, College of Physics and International Center of Future Science, Jilin University, Changchun 130012, China; [orcid.org/0000-0002-4758-5865](#)

Complete contact information is available at:

<https://pubs.acs.org/10.1021/acs.jpcc.4c00909>

Notes

The authors declare no competing financial interest.

ACKNOWLEDGMENTS

This work was supported by the National Key Research and Development Program of China (grant nos. 2021YFA1400503 and 2018YFA0703400), the Natural Science Foundation of China (grant nos. T2325013, 12074140, 52288102, and 12347162), China Postdoctoral Science Foundation (grant no. 2023M731296), and the Program for Jilin University (JLU) Science and Technology Innovative Research Team. Reported calculations utilized computing facilities at the High-Performance Computing Center of Jilin University.

REFERENCES

- (1) Mao, H.-K.; Hemley, R. J. Ultrahigh-pressure transitions in solid hydrogen. *Rev. Mod. Phys.* **1994**, *66*, 671.
- (2) Mcmillan, P. F. New materials from high-pressure experiments. *Nat. Mater.* **2002**, *1*, 19.
- (3) Mcmillan, P. F. New materials from high pressure experiments: challenges and opportunities. *High Press. Res.* **2003**, *23*, 7.
- (4) Ma, Y.; Eremets, M.; Oganov, A. R.; Xie, Y.; Trojan, I.; Medvedev, S.; Lyakhov, A. O.; Valle, M.; Prakapenka, V. Transparent dense sodium. *Nature* **2009**, *458*, 182.
- (5) Dong, X.; Oganov, A. R.; Cui, H.; Zhou, X. F.; Wang, H. T. Electronegativity and chemical hardness of elements under pressure. *Proc. Natl. Acad. Sci. U. S. A.* **2022**, *119*, No. e2117416119.
- (6) Huang, Q.; Yu, D.; Xu, B.; Hu, W.; Ma, Y.; Wang, Y.; Zhao, Z.; Wen, B.; He, J.; Liu, Z.; Tian, Y. Nanotwinned diamond with unprecedented hardness and stability. *Nature* **2014**, *510*, 250.
- (7) Zhang, L.; Wang, Y.; Lv, J.; Ma, Y. Materials discovery at high pressures. *Nat. Rev. Mater.* **2017**, *2*, 17005.
- (8) Pauling, L. The formulas of antimonic acid and the antimonates. *J. Am. Chem. Soc.* **1895**, *1933*, 55.
- (9) Bartlett, N. Xenon hexafluoroplatinate (V) $\text{Xe}^+[\text{PtF}_6]^-$. *Proc. Chem. Soc.* **1962**, *1*, 218.
- (10) Sanloup, C.; Mao, H.-K.; Hemley, R. J. High-pressure transformations in xenon hydrates. *Proc. Natl. Acad. Sci. U.S.A.* **2002**, *99*, 25.
- (11) Somayazulu, M.; Dera, P.; Goncharov, A. F.; Gramsch, S. A.; Liermann, P.; Yang, W.; Liu, Z.; Mao, H.-K.; Hemley, R. J. Pressure-induced bonding and compound formation in xenon-hydrogen solids. *Nat. Chem.* **2010**, *2*, 50.
- (12) Zhu, Q.; Jung, D. Y.; Oganov, A. R.; Glass, C. W.; Gatti, C.; Lyakhov, A. O. Stability of xenon oxides at high pressures. *Nat. Chem.* **2013**, *5*, 61.
- (13) Plisson, T.; Weck, G.; Loubeyre, P. $(\text{N}_2)_6\text{Ne}_7$: A High Pressure van der Waals Insertion Compound. *Phys. Rev. Lett.* **2014**, *113*, No. 025702.
- (14) Zhu, L.; Liu, H.; Pickard, C. J.; Zou, G.; Ma, Y. Reactions of xenon with iron and nickel are predicted in the Earth's inner core. *Nat. Chem.* **2014**, *6*, 644.
- (15) Miao, M.; Wang, X.; Brug, J.; Spera, F.; Jackson, M. G.; Kresse, G.; Lin, H. Anionic chemistry of noble gases: formation of Mg-NG (NG = Xe, Kr, Ar) compounds under pressure. *J. Am. Chem. Soc.* **2015**, *137*, 14122.
- (16) Dong, X.; Oganov, A. R.; Goncharov, A. F.; Stavrou, E.; Lobanov, S.; Saleh, G.; Qian, G.; Zhu, Q.; Gatti, C.; Deringer, V. L.; et al. A stable compound of helium and sodium at high pressure. *Nat. Chem.* **2017**, *9*, 440.
- (17) Stavrou, E.; Yao, Y.; Goncharov, A. F.; Lobanov, S. S.; Zaug, J. M.; Liu, H.; Greenberg, E.; Prakapenka, V. B. Synthesis of xenon and iron-nickel intermetallic compounds at Earth's core thermodynamic conditions. *Phys. Rev. Lett.* **2018**, *120*, No. 096001.
- (18) Zhang, J.; Lv, J.; Li, H.; Feng, X.; Lu, C.; Redfern, S. A. T.; Liu, H.; Chen, C.; Ma, Y. Rare helium-bearing compound FeO_2He stabilized at deep-earth conditions. *Phys. Rev. Lett.* **2018**, *121*, No. 255703.
- (19) Liu, C.; Gao, H.; Wang, Y.; Needs, R. J.; Pickard, C. J.; Sun, J.; Wang, H.; Xing, D. Multiple superionic states in helium-water compounds. *Nat. Phys.* **2019**, *15*, 1065.
- (20) Shi, J.; Cui, W.; Hao, J.; Xu, M.; Wang, X.; Li, Y. Formation of ammonia-helium compounds at high pressure. *Nat. Commun.* **2020**, *11*, 3164.
- (21) Gao, H.; Liu, C.; Hermann, A.; Needs, R. J.; Pickard, C. J.; Wang, H.; Sun, J. Coexistence of plastic and partially diffusive phases in a helium-methane compound. *Natl. Sci. Rev.* **2020**, *7*, 1540.
- (22) Liu, C.; Gao, H.; Hermann, A.; Wang, Y.; Miao, M.; Pickard, C. J.; Needs, R. J.; Wang, H.; Xing, D.; Sun, J. Plastic and superionic helium ammonia compounds under high pressure and high temperature. *Phys. Rev. X* **2020**, *10*, No. 021007.
- (23) Miao, M.; Sun, Y.; Liu, H.; Ma, Y. Open questions on the high-pressure chemistry of the noble gases. *Commun. Chem.* **2022**, *5*, 15.

- (24) Zhang, J.; Liu, H.; Ma, Y.; Chen, C. Direct H-He Chemical Association in Superionic $\text{FeO}_2\text{H}_2\text{He}$ at Deep-Earth Conditions. *Natl. Sci. Rev.* **2021**, 9, nwab168.
- (25) Zhang, P.; Shi, J.; Cui, W.; Liu, C.; Ding, S.; Yang, K.; Li, Y. Formation of $\text{NH}_3\text{-Xe}$ compound at the extreme condition of planetary interiors. *Phys. Rev. B* **2022**, 105, No. 214109.
- (26) Klotz, S.; Chervin, J. C.; Munsch, P.; Le marchand, G. Hydrostatic limits of 11 pressure transmitting media. *J. Phys. D: Appl. Phys.* **2009**, 42, No. 075413.
- (27) Simpson, P. D.; Monserrat, B.; Zhang, L.; Gorelli, F. Distinct vibrational signatures and complex phase behavior in metallic oxygen. *Matter Radiat. Extremes* **2024**, 9, No. 028401.
- (28) Mao, H.-K.; Hemley, R. J.; Wu, Y.; Jephcoat, A. P.; Finger, L. W.; Zha, C. S.; Bassett, W. A. High-Pressure phase diagram and equation of state of solid helium from single-crystal X-Ray diffraction to 23.3 GPa. *Phys. Rev. Lett.* **1988**, 60, 2649.
- (29) Dewaele, A.; Loubeyre, P. Pressurizing conditions in helium-pressure-transmitting medium. *High Press. Res.* **2007**, 27, 419.
- (30) Errandonea, D.; Muñoz, A.; Gonzalez-platas, J. Comment on "High-pressure x-ray diffraction study of $\text{YBO}_3/\text{Eu}^{3+}$, GdBO_3 , and EuBO_3 : Pressure-induced amorphization in GdBO_3 ". *J. Appl. Phys.* **2014**, 115, 216101.
- (31) Ruoff, A. L.; Luo, H. Pressure strengthening: A possible route to obtaining 9 Mbar and metallic diamonds. *J. Appl. Phys.* **1991**, 70, 2066.
- (32) Merkel, S.; Hemley, R. J.; Mao, H.-K. Finite-element modeling of diamond deformation at multimegarbar pressures. *Appl. Phys. Lett.* **1999**, 74, 656.
- (33) Eggert, J. H.; Goettel, K. A.; Silvera, I. F. Ruby at high pressure. I. Optical line shifts to 156 GPa. *Phys. Rev. B* **1989**, 40, 5724.
- (34) Takemura, K. Evaluation of the hydrostaticity of a helium-pressure medium with powder x-ray diffraction techniques. *J. Appl. Phys.* **2001**, 89, 662.
- (35) Libotte, H.; Gaspard, J. P. Pressure-induced distortion of the β -Sn phase of silicon: Effects of nonhydrostaticity. *Phys. Rev. B* **2000**, 62, 7110.
- (36) Von barge, N.; Boehler, R. Effect of non-hydrostaticity on the α - ϵ transition of iron. *High Press. Res.* **1990**, 6, 133.
- (37) Deemyad, S.; Tomita, T.; Hamlin, J. J.; Beckett, B. R.; Schilling, J. S.; Hinks, D. G.; Jorgensen, J. D.; Lee, S.; Tajim, S. Dependence of the superconducting transition temperature of single and polycrystalline MgB_2 on hydrostatic pressure. *Phys. C: Supercond.* **2003**, 385, 105.
- (38) Singh, A. K.; Mao, H.-K.; Shu, J.; Hemley, R. J. Estimation of single-crystal elastic moduli from polycrystalline X-Ray diffraction at high pressure: application to FeO and Iron. *Phys. Rev. Lett.* **1998**, 80, 2157.
- (39) Mao, H.-K.; Badro, J.; Shu, J.; Hemley, R. J.; Singh, A. K. Strength, anisotropy, and preferred orientation of solid argon at high pressures. *J. Phys.: Condens Matter* **2006**, 18, S963.
- (40) Kresse, G.; Furthmüller, J. Efficient iterative schemes for ab initio total-energy calculations using a plane-wave basis set. *Phys. Rev. B* **1996**, 54, 11169.
- (41) Perdew, J. P.; Burke, K.; Ernzerhof, M. Generalized gradient approximation made simple. *Phys. Rev. Lett.* **1996**, 77, 3865.
- (42) Monkhorst, H. J.; Pack, J. D. Special points for Brillouin-zone integrations. *Phys. Rev. B* **1976**, 13, 5188.
- (43) Togo, A.; Oba, F.; Tanaka, I. First-principles calculations of the ferroelastic transition between rutile-type and CaCl_2 -type SiO_2 at high pressures. *Phys. Rev. B* **2008**, 78, No. 134106.
- (44) Hill, R. The elastic behaviour of a crystalline aggregate. *Proc. Phys. Soc. London, Sect. A* **1952**, 65, 349.
- (45) Liu, C.; Song, X.; Li, Q.; Ma, Y.; Chen, C. Smooth flow in diamond: atomistic ductility and electronic conductivity. *Phys. Rev. Lett.* **2019**, 123, No. 195504.
- (46) Liu, C.; Song, X.; Li, Q.; Ma, Y.; Chen, C. Superconductivity in compression-shear deformed diamond. *Phys. Rev. Lett.* **2020**, 124, No. 147001.
- (47) Liang, H.; Li, H. F.; Li, Q.; Chen, C. Toughening a superstrong carbon crystal: sequential bond-breaking mechanisms. *Phys. Rev. B* **2020**, 102, No. 134105.
- (48) Liang, H.; Li, Q.; Chen, C. Atomistic mechanisms for contrasting stress-strain relations of B_{13}CN and B_{13}C_2 . *J. Phys. Chem. Lett.* **2020**, 11, 10454–10462.
- (49) Liu, C.; Song, X.; Li, Q.; Ma, Y.; Chen, C. Superconductivity in shear strained semiconductors. *Chin. Phys. Lett.* **2021**, 138, No. 086301.
- (50) Song, X.; Liu, C.; Li, Q.; Ma, Y.; Chen, C. Intrinsic dense twinning via release of native strain. *Acta Mater.* **2023**, 257, No. 119151.
- (51) Liang, H.; Wang, D.; Song, X.; Guo, Q.; Li, Q. Structural and stress response of nanotwinned B_{13}CN under large strains. *J. Phys. Chem. Lett.* **2023**, 14, 10475.
- (52) Min, N.; Liang, H.; Chen, H.; Song, X.; Zhou, D.; Li, Q. Theoretical design of superhard twinned BC_2N . *Scr. Mater.* **2024**, 240, No. 115843.
- (53) Grimvall, G.; Magyari-köpe, B.; Ozoliņš, V.; Persson, K. A. Lattice instabilities in metallic elements. *Rev. Mod. Phys.* **2012**, 84, 945.
- (54) Finger, L. W.; Hazen, R. M.; Zou, G.; Mao, H.-K.; Bell, P. M. Structure and compression of crystalline argon and neon at high pressure and room temperature. *Appl. Phys. Lett.* **1981**, 39, 892.
- (55) Errandonea, D.; Schwager, B.; Boehler, R. Crystal structure transformations of rare-gas solids under pressure. *High Press. Res.* **2002**, 22, 375.
- (56) Loubeyre, P.; Letoullec, R.; Pinceaux, J. P.; Mao, H.-K.; Hu, J.; Hemley, R. J. Equation of state and phase diagram of solid He from single-crystal X-ray diffraction over a large P-T domain. *Phys. Rev. Lett.* **1993**, 71, 2272.
- (57) Khairallah, S. A.; Militzer, B. First-principles studies of the metallization and the equation of state of solid helium. *Phys. Rev. Lett.* **2008**, 101, No. 106407.
- (58) Hemley, R. J.; Zha, C. S.; Jephcoat, A. P.; Mao, H.-K.; Finger, L. W.; Cox, D. E. X-ray diffraction and equation of state of solid neon to 110 GPa. *Phys. Rev. B* **1989**, 39, 11820.
- (59) Dewaele, A.; Datchi, F.; Loubeyre, P.; Mezouar, M. High pressure-high temperature equations of state of neon and diamond. *Phys. Rev. B* **2008**, 77, No. 094106.
- (60) He, Y.; Tang, X.; Pu, Y. First-principle study of solid neon under high compression. *Physica B* **2010**, 405, 4335.
- (61) McMahan, A. K. Structural transitions and metallization in compressed solid argon. *Phys. Rev. B* **1986**, 33, 5344.
- (62) Kwon, I.; Collins, L. A.; Kress, J. D.; Troullier, N. First-principles study of solid Ar and Kr under high compression. *Phys. Rev. B* **1995**, 52, 15165.
- (63) Errandonea, D.; Boehler, R.; Japel, S.; Mezouar, M.; Benedetti, L. R. Structural transformation of compressed solid Ar: An x-ray diffraction study to 114 GPa. *Phys. Rev. B* **2006**, 73, No. 092106.
- (64) Jephcoat, A. P.; Mao, H.-K.; Finger, L. W.; Cox, D. E.; Hemley, R. J.; Zha, C. S. Pressure-induced structural phase transitions in solid xenon. *Phys. Rev. Lett.* **1987**, 59, 2670.
- (65) Goettel, K. A.; Eggert, J. H.; Silvera, I. F. Optical evidence for the metallization of xenon at 132(5) GPa. *Phys. Rev. Lett.* **1989**, 62, 665.
- (66) Reichlin, R.; Brister, K. E.; McMahan, A. K.; Ross, M.; Martin, S.; Vohra, Y. K.; Ruoff, A. L. Evidence for the insulator-metal transition in xenon from optical, X-Ray, and band-structure studies to 170 GPa. *Phys. Rev. Lett.* **1989**, 62, 669.
- (67) Eremets, M. I.; Gregoryanz, E. A.; Struzhkin, V. V.; Mao, H. K.; Hemley, R. J.; Mulders, N.; Zimmerman, N. M. Electrical conductivity of xenon at megabar pressures. *Phys. Rev. Lett.* **2000**, 85, 2797.
- (68) Cynn, H.; Yoo, C. S.; Baer, B.; Iota-herbei, V.; McMahan, A. K.; Nicol, M.; Carlson, S. Martensitic fcc-to-hcp transformation observed in xenon at high pressure. *Phys. Rev. Lett.* **2001**, 86, 4552.
- (69) *Supplemental Material*.
- (70) Freiman, Y. A.; Tretyak, S. M.; Grechnev, A.; Goncharov, A. F.; Tse, J. S.; Errandonea, D.; Mao, H.-K.; Hemley, R. J. Lattice distortion

of hcp solid helium under pressure. *Phys. Rev. B* **2009**, *80*, No. 094112.

(71) Teter, D. M. Computational alchemy: the search for new superhard materials. *MRS Bull.* **1998**, *23*, 22.

(72) Takemura, K. Hydrostaticity in high pressure experiments: some general observations and guidelines for high pressure experimenters. *High Press. Res.* **2021**, *41*, 155.

(73) Song, X.; Liu, C.; Li, Q.; Hemley, R. J.; Ma, Y.; Chen, C. Stress-induced high-T_c superconductivity in solid molecular hydrogen. *Proc. Natl. Acad. Sci. U. S. A.* **2022**, *119*, No. e212269111.

(74) Ogata, S.; Li, J.; Yip, S. Ideal pure shear strength of aluminum and copper. *Science* **2002**, *298*, 807.

(75) Roundy, D.; Cohen, M. L. Ideal strength of diamond, Si, and Ge. *Phys. Rev. B* **2001**, *64*, No. 212103.

Unexpected Strength of Noble Gas Solids in Diamond Anvil Cells

Hui Liang,^a Nan Min,^{a,b} Di Wang,^{a,b} Xianqi Song,^{a,b} Penyue Gao,^{a*} and Quan Li,^{a,b*}

^a State Key Lab of Superhard Materials, and Key Laboratory of Material Simulation Methods & Software of Ministry of Education, College of Physics, Jilin University, Changchun 130012, China

^b International Center of Future Science, Jilin University, Changchun 130012, China

*Corresponding author.

Email address: gpy@calypso.cn(P. Y. Gao); liquan777@jlu.edu.cn (Q. Li).

This file includes:

Table S1, S2

Figures S1-S11

Table S1. Lattice parameters (\AA) and volumes (cm^3/mol) of NG solids calculated using the GGA functional compared with experimental data.

	He (15 GPa)			Ne (5 GPa)			Ar (5 GPa)			Kr (50 GPa)			Xe (5 GPa)		
	hcp			fcc			fcc			hcp			fcc		
	<i>a</i>	<i>c</i>	<i>V</i>	<i>a</i>	<i>V</i>	<i>a</i>	<i>V</i>	<i>a</i>	<i>V</i>	<i>a</i>	<i>c</i>	<i>a</i>	<i>a</i>	<i>c</i>	
Theo.	2.083	3.399	3.844	3.798	8.243	4.746	16.091	4.233	2.991	4.890	5.529	3.909	6.385		
Exp.	2.100 ^[a]	3.430 ^[a]	3.944 ^[a]	3.786 ^[b]	8.171 ^[b]	4.667 ^[b]	15.310 ^[b]	4.151 ^[c]	2.927 ^[c]	4.795 ^[c]	5.487 ^[c]	3.857 ^[c]	6.367 ^[c]		

^[a] Reference [1]

^[b] Reference [2]

^[c] Reference [3]

Table S2. Calculated Elastic Parameters (C_{ij}) of NG solids at 200 GPa (all in GPa)

	C_{11}	C_{12}	C_{13}	C_{33}	C_{44}
He	624.2	257.9	125.8	746.1	177.4
Ne	624.4	429.1			341.9
Ar	592.6	339.1			367.4
Kr	887.6	318.3	170.3	1011.7	189.7
Xe	821.2	276.7	137.5	1028.7	199.5

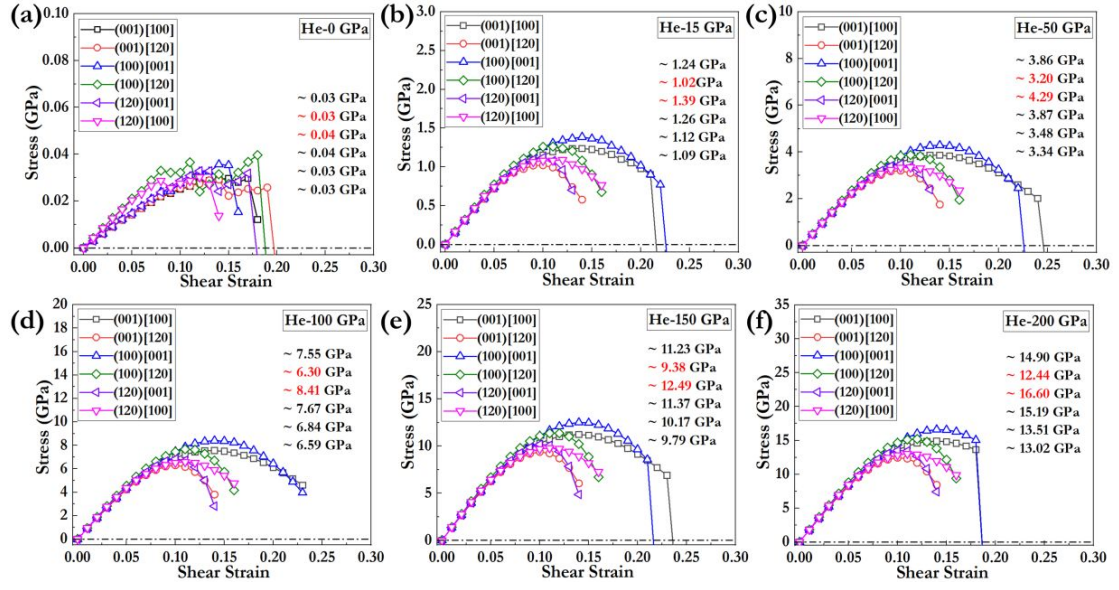


Fig. S1. Stress-strain relations of solid He under shear strains along various indicated crystallographic directions at hydrostatic pressures of 0, 15, 50, 100, 150, and 200 GPa.

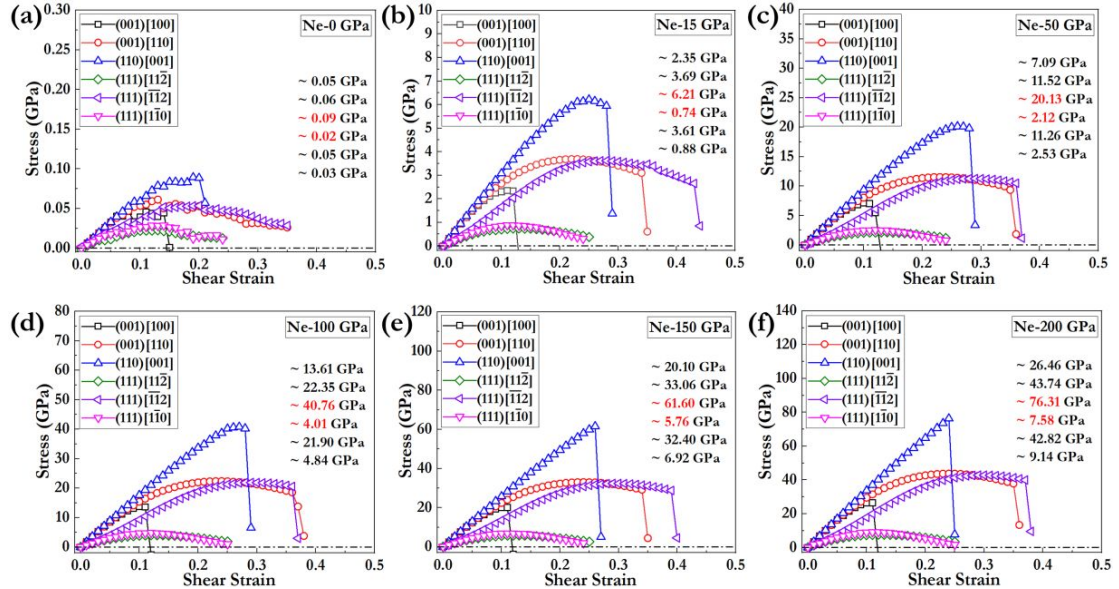


Fig. S2. Stress-strain relations of solid Ne under shear strains along various indicated crystallographic directions at hydrostatic pressures of 0, 15, 50, 100, 150, and 200 GPa.

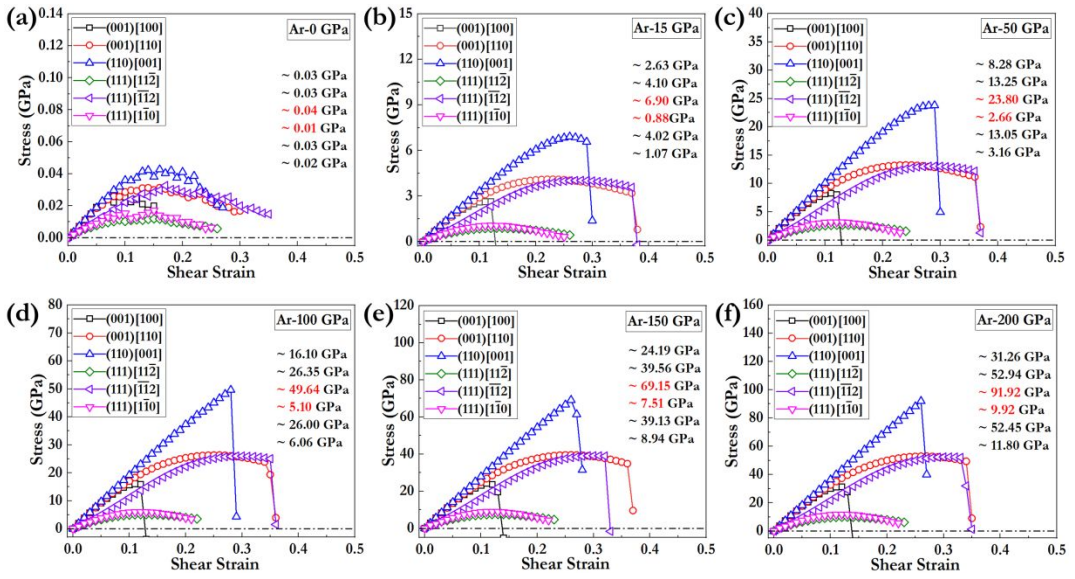


Fig. S3. Stress-strain relations of solid Ar under shear strains along various indicated crystallographic directions at hydrostatic pressures of 0, 15, 50, 100, 150, and 200 GPa.

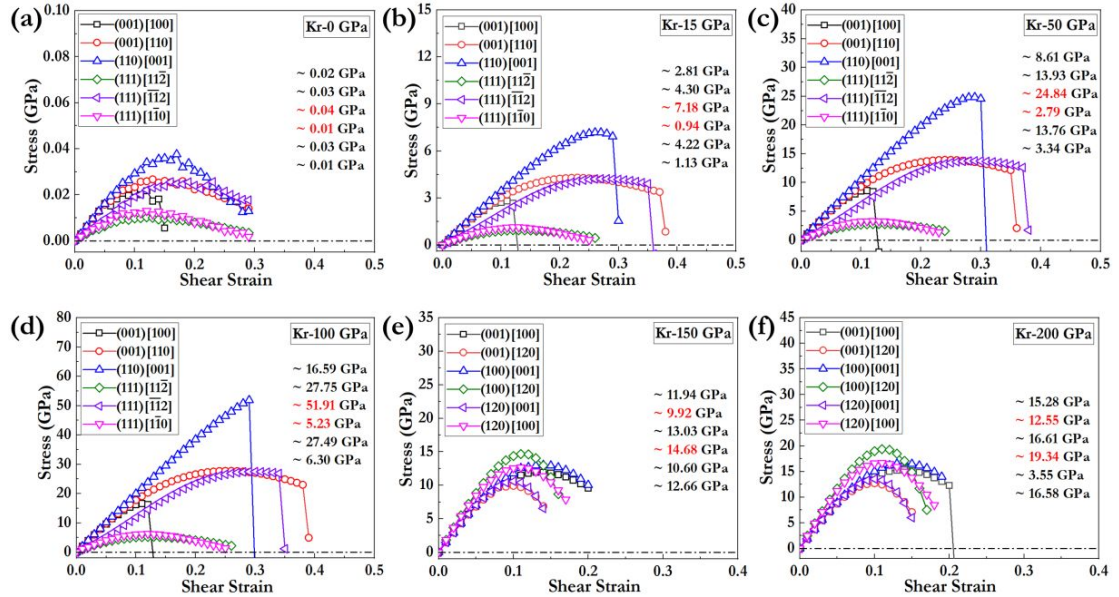


Fig. S4. Stress-strain relations of solid Kr under shear strains along various indicated crystallographic directions at hydrostatic pressures of 0, 15, 50, 100, 150, and 200 GPa.

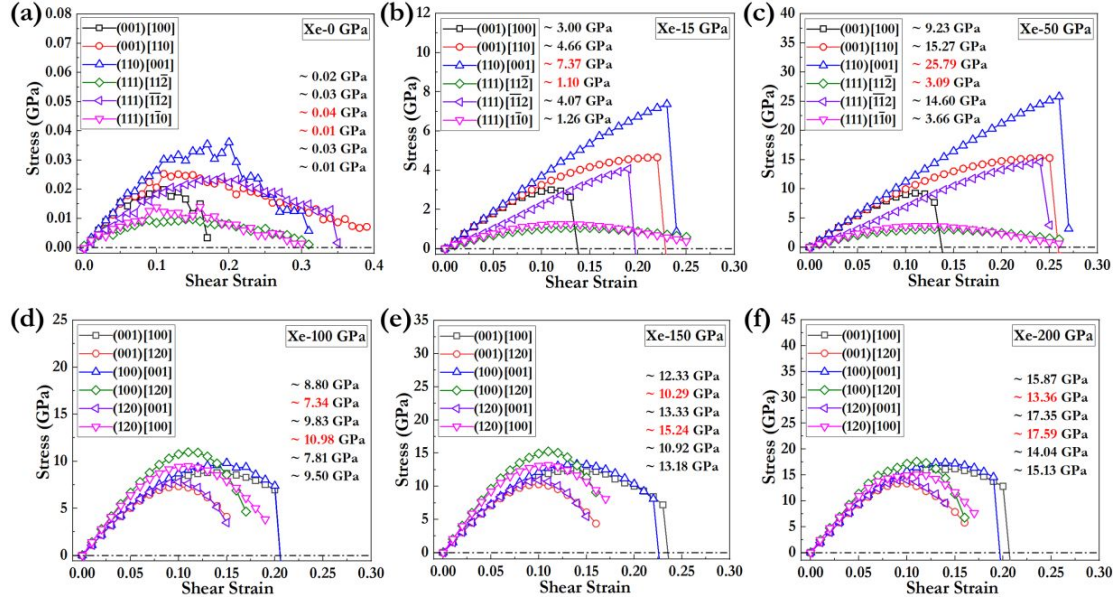


Fig. S5. Stress-strain relations of solid Xe under shear strains along various indicated crystallographic directions at hydrostatic pressures of 0, 15, 50, 100, 150, and 200 GPa.

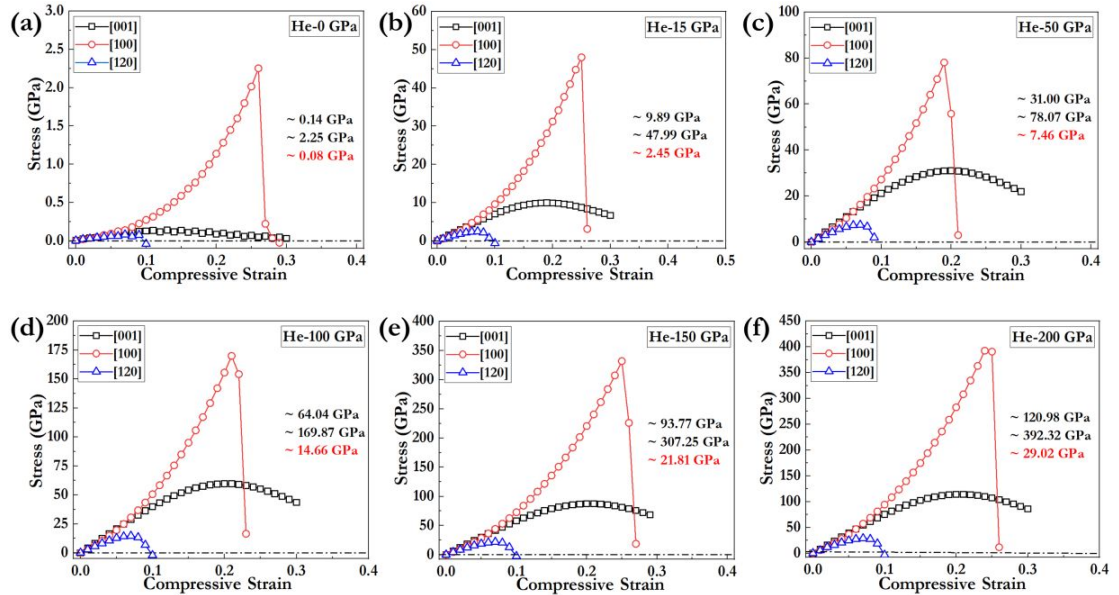


Fig. S6. Stress-strain relations of solid He under compressive strains along various indicated crystallographic directions at hydrostatic pressures of 0, 15, 50, 100, 150, and 200 GPa.

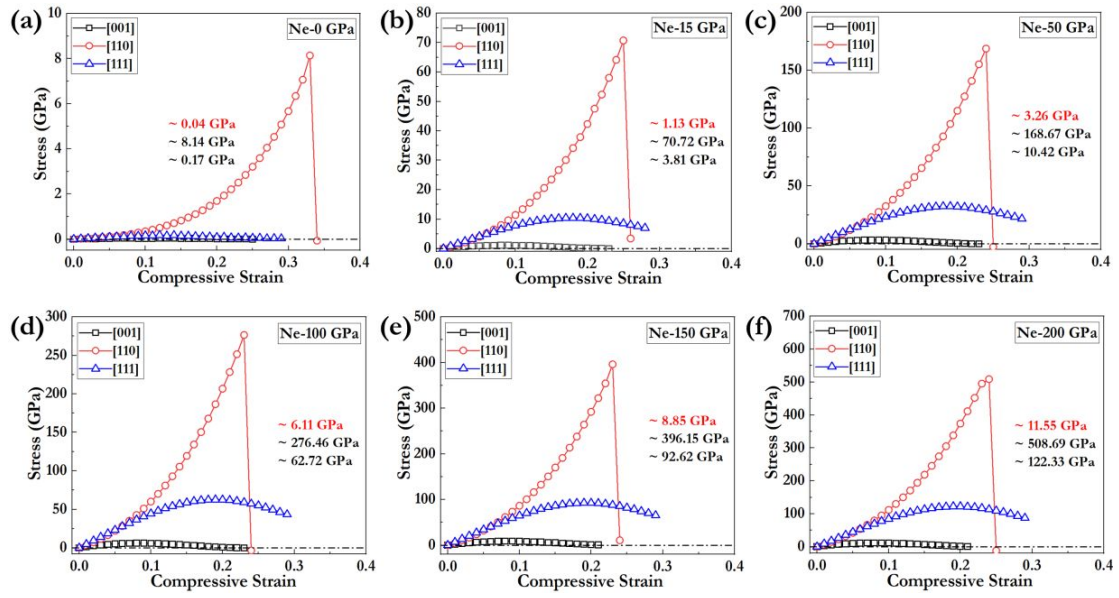


Fig. S7. Stress-strain relations of solid Ne under compressive strains along various indicated crystallographic directions at hydrostatic pressures of 0, 15, 50, 100, 150, and 200 GPa.

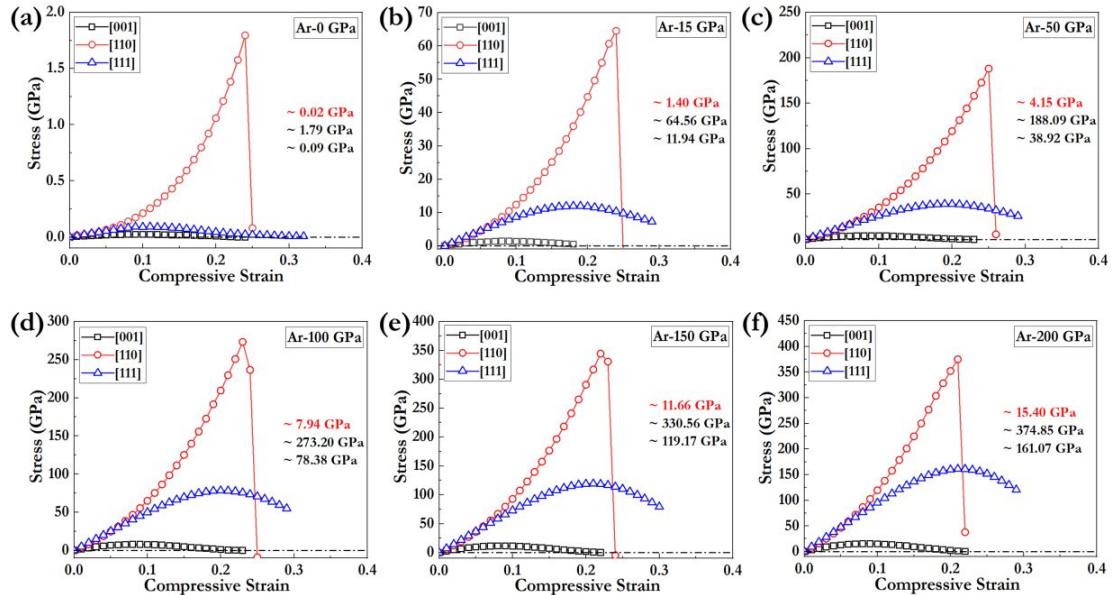


Fig. S8. Stress-strain relations of solid Ar under compressive strains along various indicated crystallographic directions at hydrostatic pressures of 0, 15, 50, 100, 150, and 200 GPa.

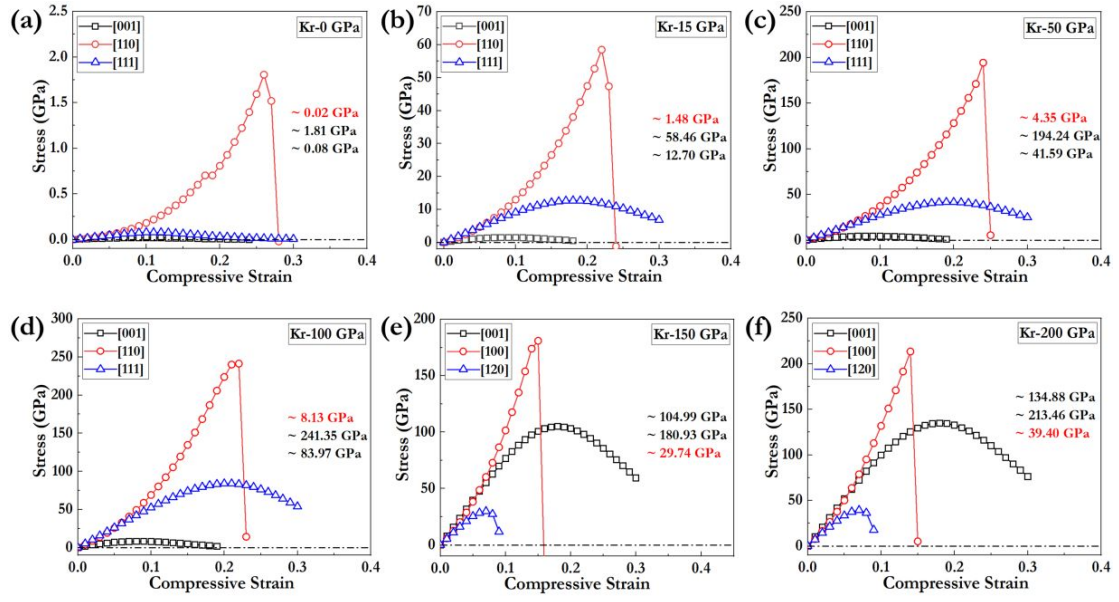


Fig. S9. Stress-strain relations of solid Kr under compressive strains along various indicated crystallographic directions at hydrostatic pressures of 0, 15, 50, 100, 150, and 200 GPa.

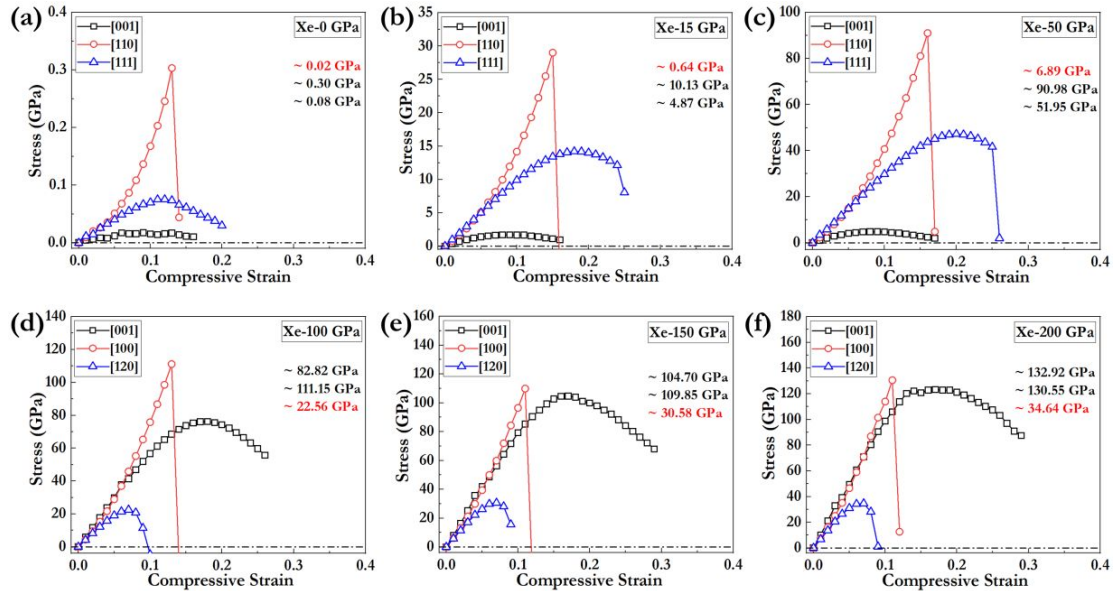


Fig. S10. Stress-strain relations of solid Xe under compressive strains along various indicated crystallographic directions at hydrostatic pressures of 0, 15, 50, 100, 150, and 200 GPa.

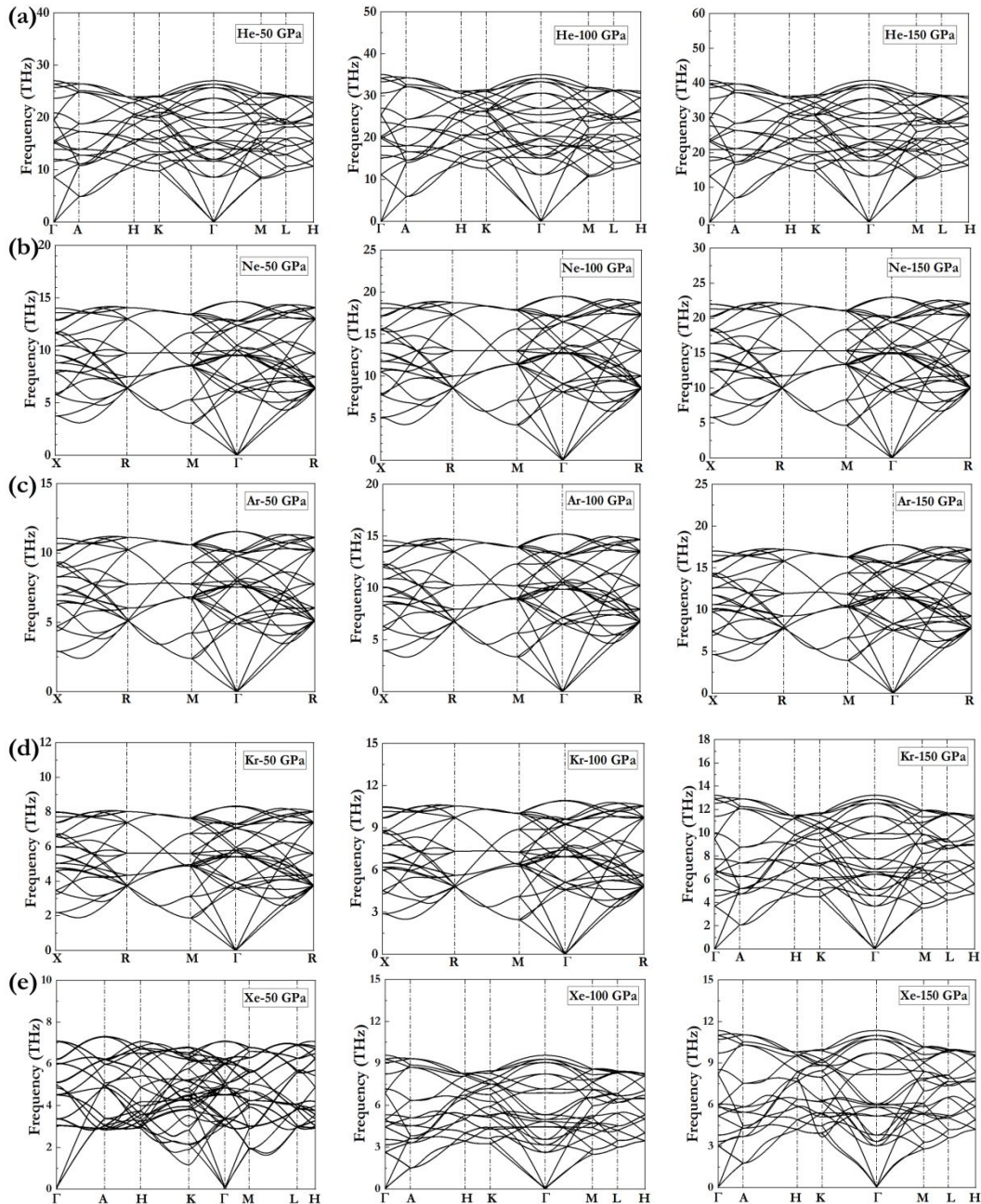


Fig. S11. Phonon dispersions curves of solid He, Ne, Ar, Kr, and Xe at hydrostatic pressures of 50, 100, and 150.

REFERENCES

- (1) Mao, H.K.; Hemley, R.J.; Wu, Y.; Jephcoat, A.P.; Finger, L.W.; Zha, C.S.; Bassett, W.A. High-Pressure phase diagram and equation of state of solid helium from single-crystal X-Ray diffraction to 23.3 GPa. *Phys. Rev. Lett.* **1988**, *60*, 2649.
- (2) Finger, L. W.; Hazen, R.M.; Zou, G.; Mao, H.K.; Bell, P.M. Structure and compression of crystalline argon and neon at high pressure and room temperature. *Appl. Phys. Lett.* **1981**, *39*, 892.

- (3) Errandonea, D.; Schwager, B.; and Boehler, R. Crystal structure transformations of rare-gas solids under pressure. *High Press. Res.* **2002**, *22*, 375.